



Navier-Stokes Simulation of UH-60A Rotor/Wake Interaction Using Adaptive Mesh Refinement

Neal M. Chaderjian
NASA Ames Research Center
Moffett Field, CA 94035



Advanced Modeling and
Simulation Seminar Series
May 18, 2017



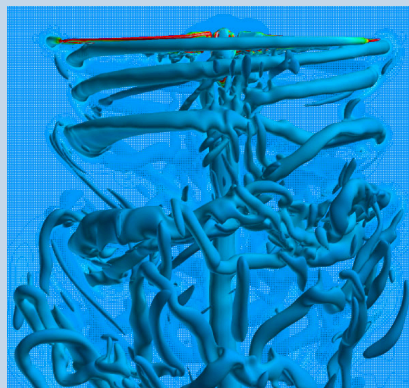
Motivation



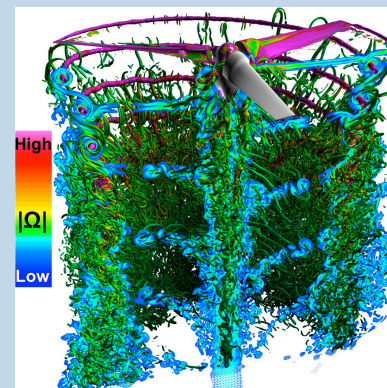
- Average CFD FM accuracy was 2.4% (2009)
 - ❖ It was believed that poor rotor wake resolution was responsible
 - ❖ This led to research in off-body (OB) adaptive mesh refinement (AMR)
- In 2011 (Chaderjian/Buning): CFD FM predicted with 0.2% for V22 TRAM
 - ❖ Vortex wake resolution had no effect (10%, 5%, and 2.5% c_{tip})
 - ❖ Rather, it was crucial to
 - Adequately resolve the formation of the blade-tip vortex
 - ❖ Fine surface mesh near rotor tip and high-order spatial accuracy
 - Maintain a physically realistic turbulent eddy viscosity in the vortex wake
 - ❖ Detached eddy simulation (DES) turbulent length scale



Coarse Wake-Grid
Resolution
 $\Delta S = 10\% c_{tip}$



No Difference
In the FM



Fine Wake-Grid
Resolution
 $\Delta S = 2.5\% c_{tip}$

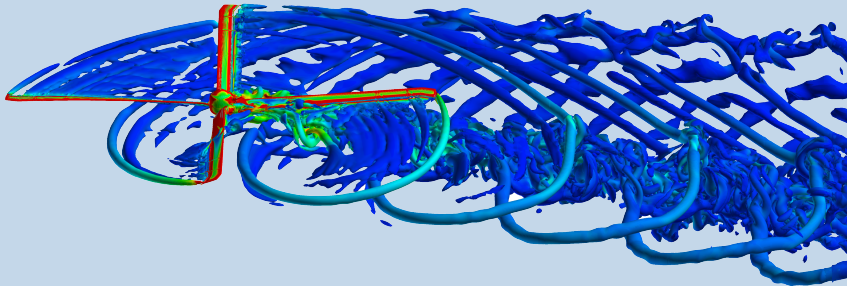


Motivation

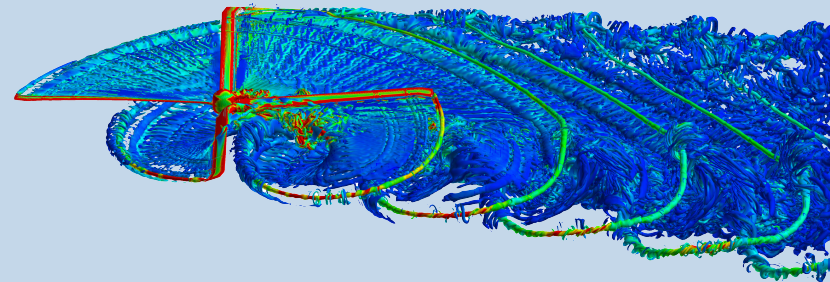


- In 2012 (Chaderjian/Ahmad): UH-60A rotor in hover and forward flight (C8534)
 - ❖ Airloads did not depend on rotor wake resolution
- **Both studies did not involve significant blade/wake interaction**

Coarse Wake-Grid
Resolution
 $\Delta S = 10\%c_{tip}$



Fine Wake-Grid
Resolution
 $\Delta S = 2.5\%c_{tip}$





Objective



- **An important question remains**
 - ❖ How are the forward-flight CFD airloads affected by rotor-wake resolution when there is significant blade/wake interaction?
 - ❖ Practical engineering issue: High resolution wakes are too expensive for most engineering applications today
- Two examples for a UH-60A rotor in forward flight are examined
 - ❖ Blade vortex interaction (BVI), flight-test counter C8513
 - ❖ Dynamic stall with BVI, flight-test counter C9017
- Also examine the physics of 2D and 3D dynamic stall
 - ❖ Discuss similarities and differences in 2D and 3D dynamic stall

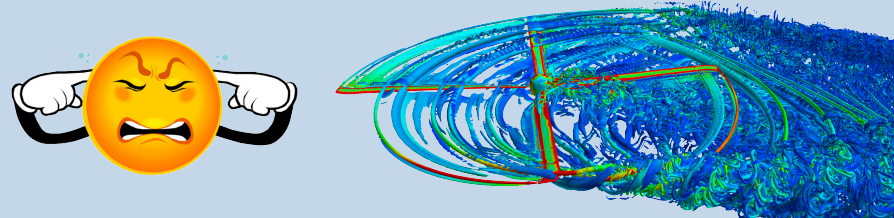


What is BVI and Dynamic Stall?



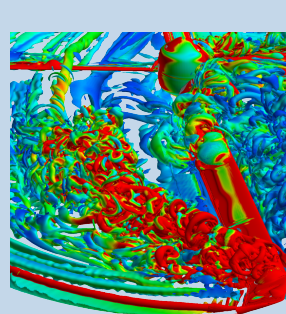
- **Blade vortex Interaction (BVI)**

- ❖ When a rotor blade interacts with the tip vortices from the other rotor blades
- ❖ Often produces high and irritating sound levels



- **Dynamic stall**

- ❖ When the required thrust exceeds what the rotor can provide
- ❖ Loss of Thrust (stall) and increased vibration
- ❖ Usually occurs at high flight speeds or load conditions
 - Limits vehicle flight speed, payload capacity, and maneuverability





Outline

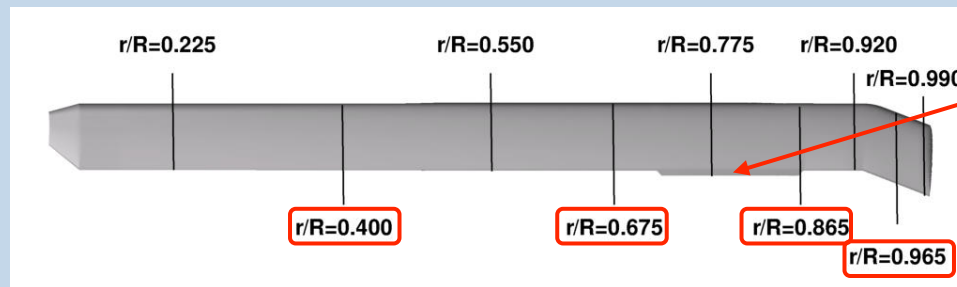
- **Flight-Test Data**
- Numerical Approach
- Numerical Results
 - ❖ BVI – UH-60A (C8513)
 - ❖ Dynamic stall
 - 2D NACA 0012 example
 - 3D UH-60A (C9017)
- Concluding Remarks



Flight-Test Data/CFD Validation



- Joint NASA/U.S. Army UH-60A Airloads Database (1993/1994)
 - ❖ Airloads at various radial locations along the rotor blade
- Bousman's qualitative analysis of dynamic stall (AHS Journal/Oct. 1998)
 - ❖ He examined the time history of blade pressures to judge when
 - Moment stall: Formation of dynamic stall vortex at blade leading edge
 - Lift stall: When dynamic stall vortex passes over blade trailing edge
 - Flow separation at blade trailing edge



Trim Tab



Outline

- Flight-Test Data
- **Numerical Approach**
- Numerical Results
 - ❖ BVI – UH-60A (C8513)
 - ❖ Dynamic stall
 - 2D example
 - 3D UH-60A (C9017)
- Concluding Remarks



Numerical Approach (CFD/CSD Loose Coupling)

Loose
Coupling
Every
¼ revolution

OVERFLOW 2.2L – CFD Flow Solver

- Solves the time-dependent Navier-Stokes equations
 - ❖ Structured overset grids
 - ❖ **2nd-order** dual time accuracy ($\Delta t = \frac{1}{4}^\circ$ rotation, 60 subiterations)
 - At least 2.3 subiteration residual drop for all grids
 - ❖ **5th-order** spatial accuracy (central differences/artificial dissipation)
 - ❖ **Hybrid RANS/LES** turbulence model
 - Spalart-Allmaras one-equation turbulence model
 - DDES length scale
 - SARC rotation/curvature correction
 - $Y^+ < 1$ at body surfaces

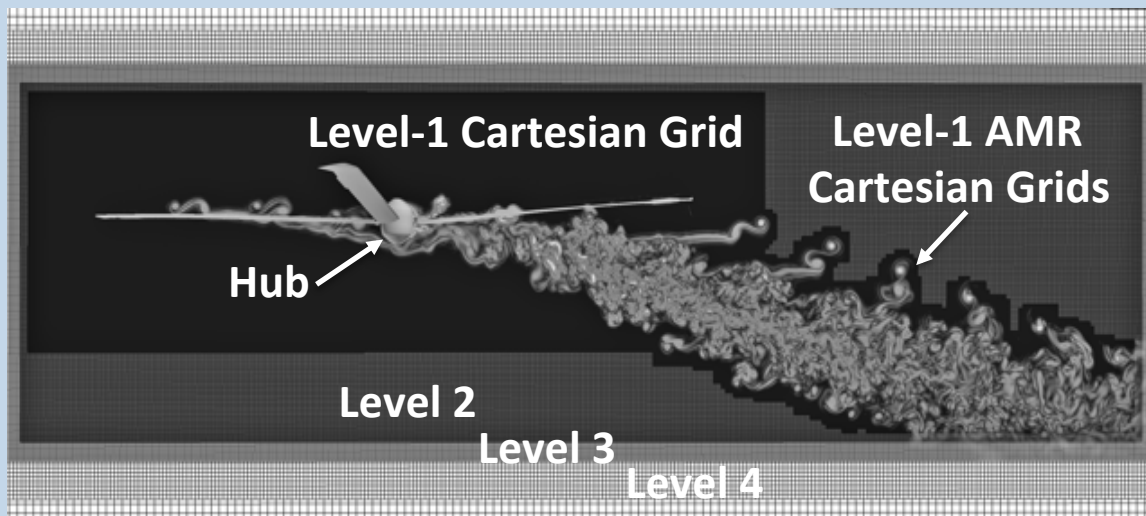
CAMRAD II – Helicopter Comprehensive Analysis Code

- Provides rotor-blade aeroelastic deflections
- Provides trim control angles at the blade root

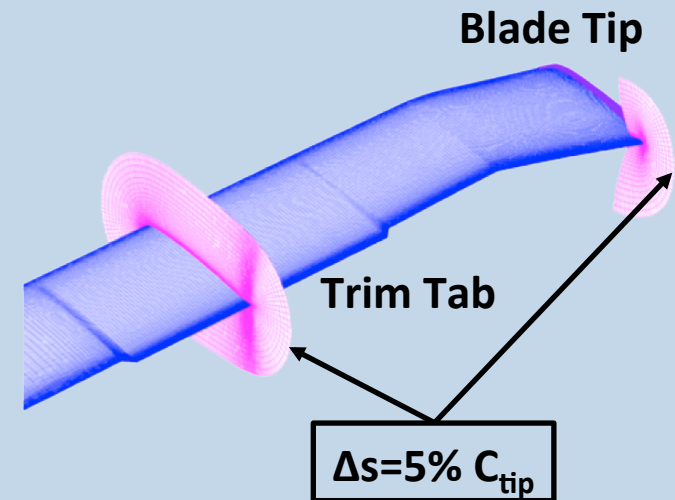


Numerical Approach (Near-Body and Off-Body Grids)

Cartesian Off-Body Grids



Rotor-Blade Grids

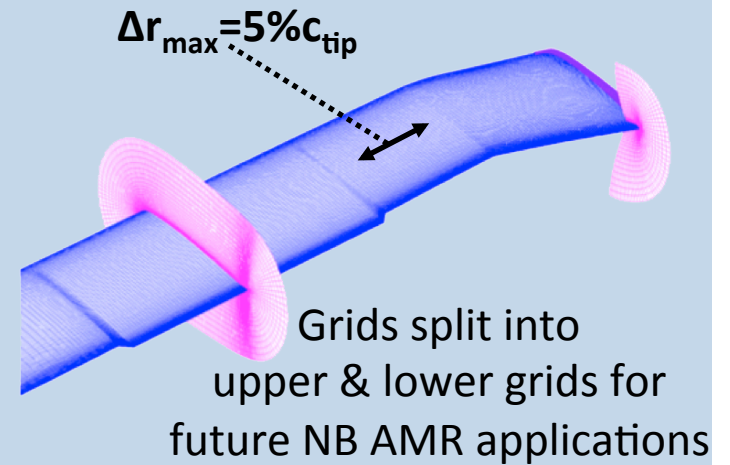
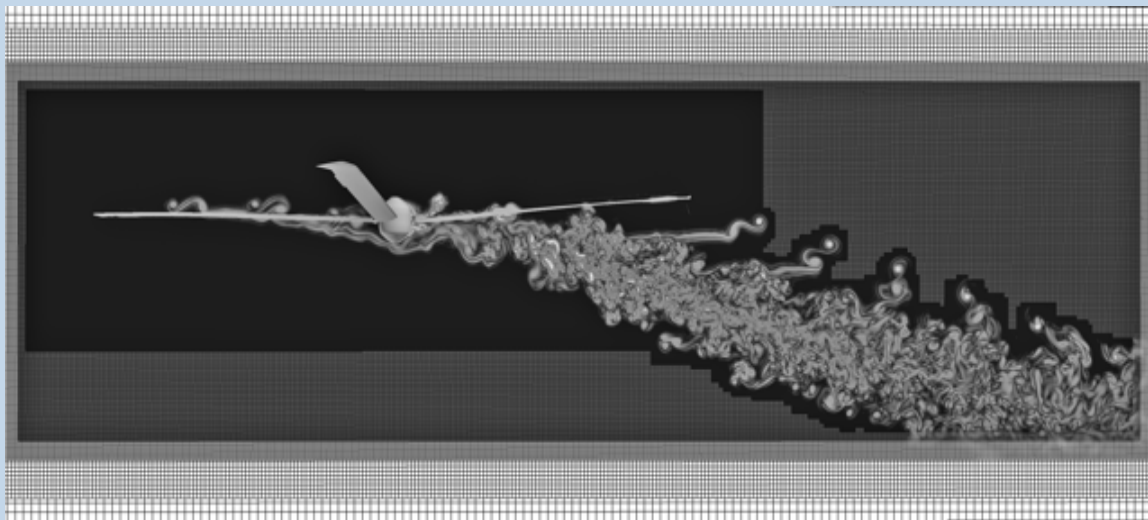


- Rotor blades/Hub use O-mesh topology
- Off-body grids use Cartesian grids with adaptive mesh refinement (AMR)
- Rotor wake captured **only with** Level-1 grids (10%, 5%, and 2.5% c_{tip})
- No interpolation throughout the resolved rotor wake
 - ❖ Has same resolution and coincident overlapping grid points



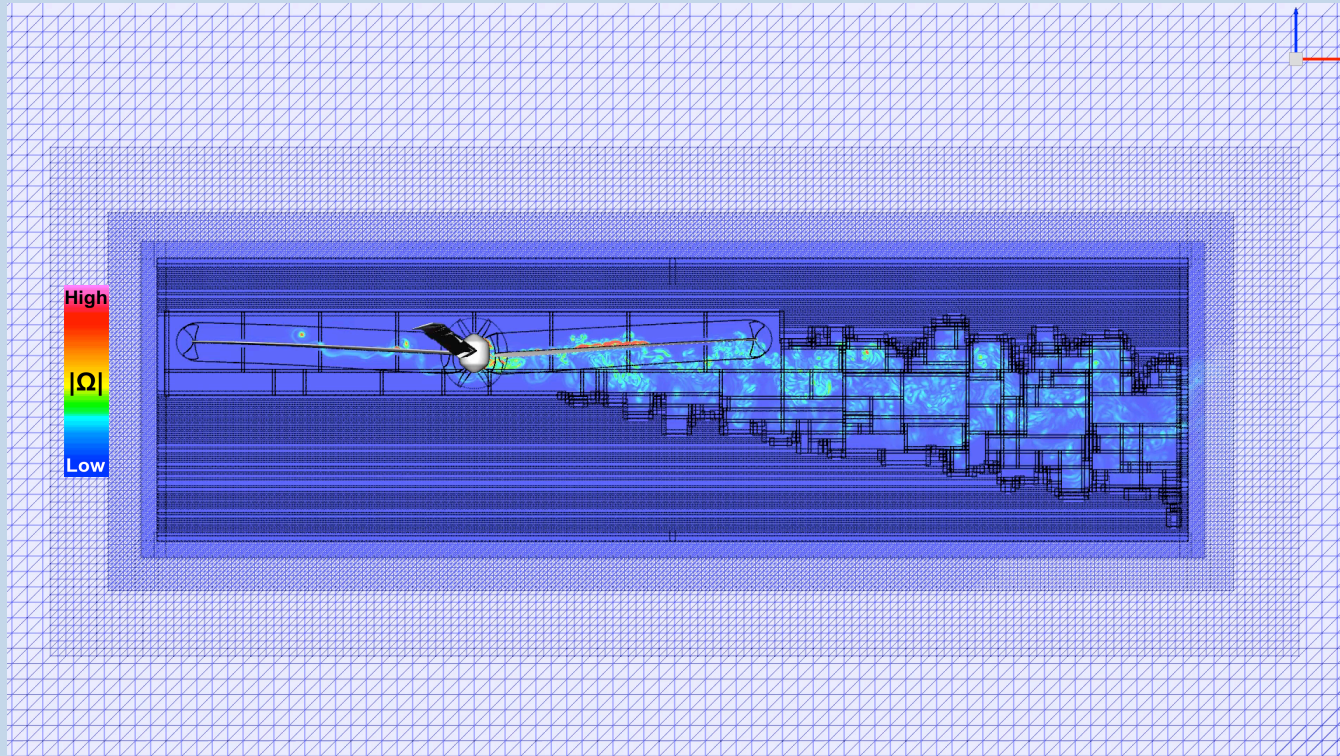
Numerical Approach (Overset Grid Statistics)

Grid Type	Number of Grids	Surface Grid Points	Volume Grid Points
Rotor Blade	4	117,763	11.8 million
Rotor Hub	3	28,875	2.5 million
Total (Near/Off-Body)	750-14,700	499,927	83 million – 1.8 billion





Numerical Approach (Off-Body AMR Bounding Boxes – Dynamic Stall)





Outline

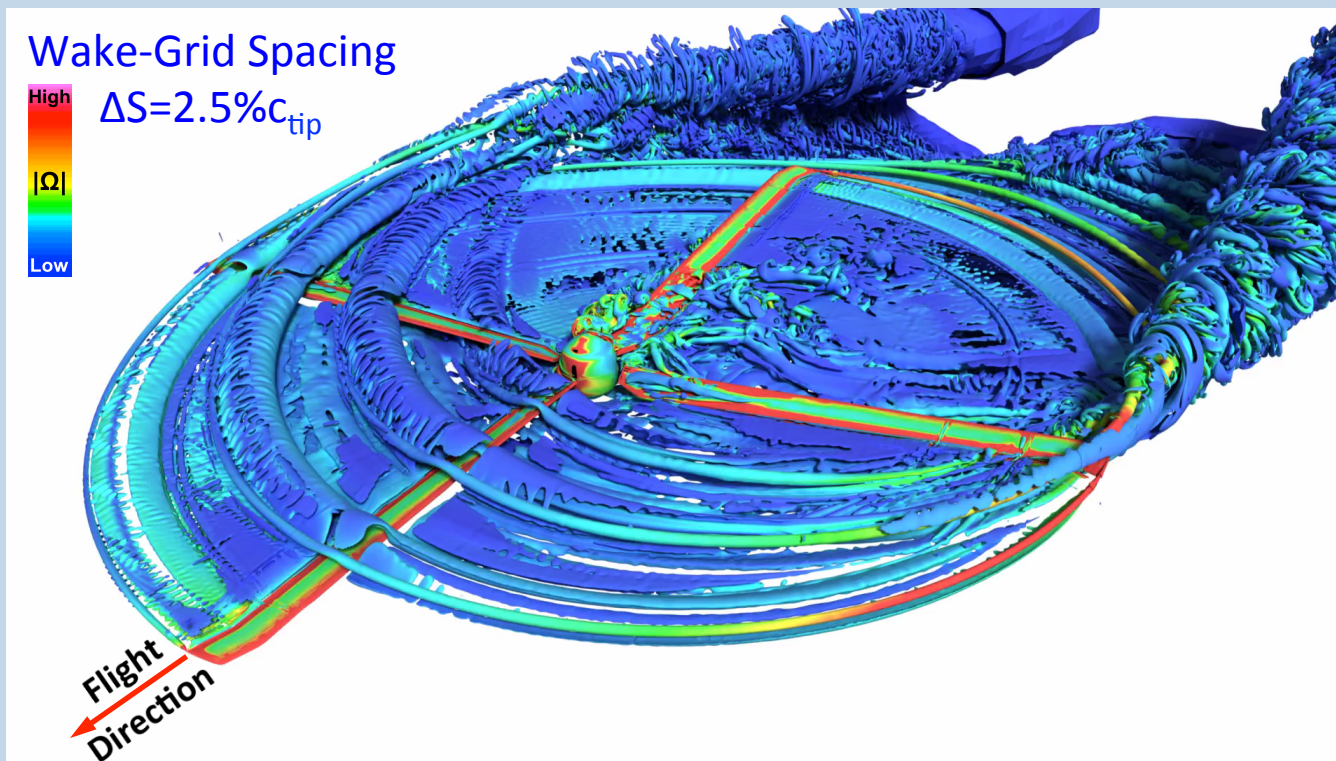
- Flight-Test Data
- Numerical Approach
- Numerical Results
 - ❖ **BVI – UH-60A (C8513)**
 - ❖ Dynamic stall
 - 2D example
 - 3D UH-60A (C9017)
- Concluding Remarks



BVI Flight Counter C8513 NASA'S OVERFLOW Navier-Stokes CFD Code



M_∞	M_{tip}	μ	Re_{tip}	a_{shaft}, deg	b, deg	C_T
0.0982	0.643	0.153	7.15×10^6	0.75	7.71	0.00675

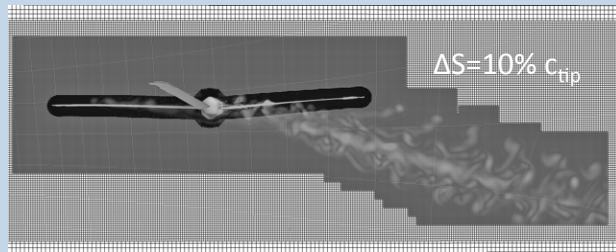




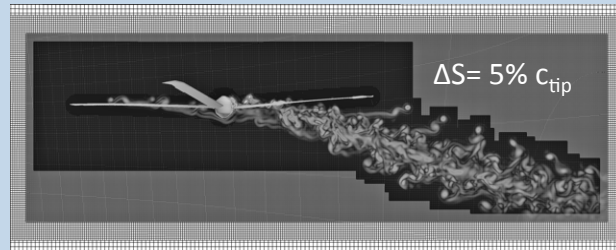
Three AMR Wake-Grid Resolutions

BVI Flight Counter C8513

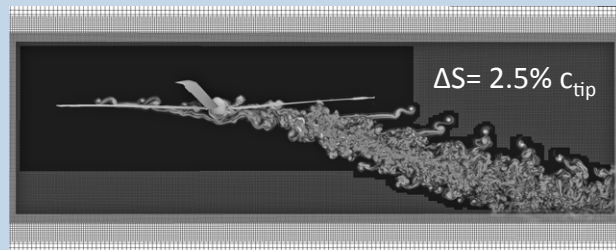
NASA's Pleiades Supercomputer
5,628 Broadwell CPU Cores



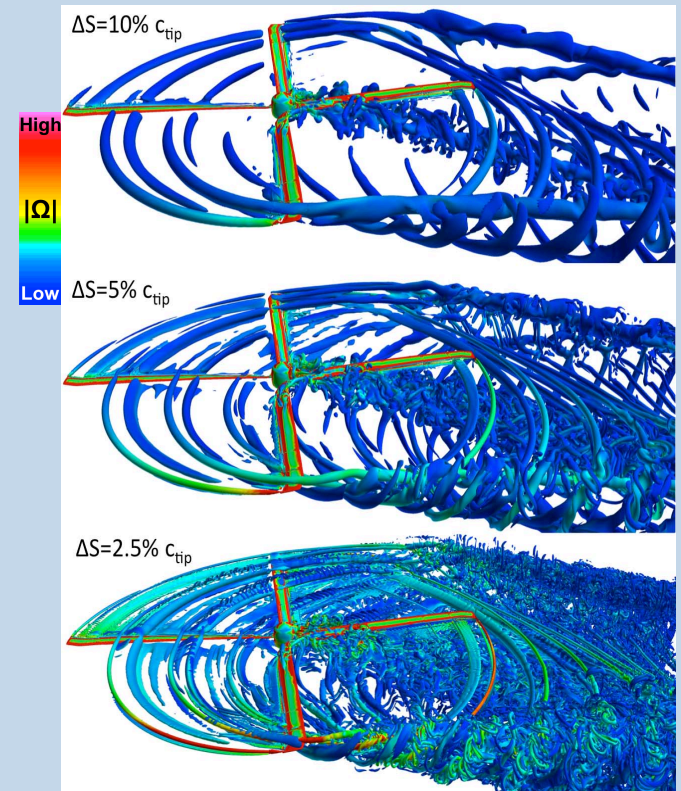
500 Grids
87 Million Grid Points
4.6 Hr/Rev



2,500 Grids
297 Million Grid Points
7.8 Hr/Rev



12,000 Grids
1.8 Billion Grid Points
40 Hr/Rev





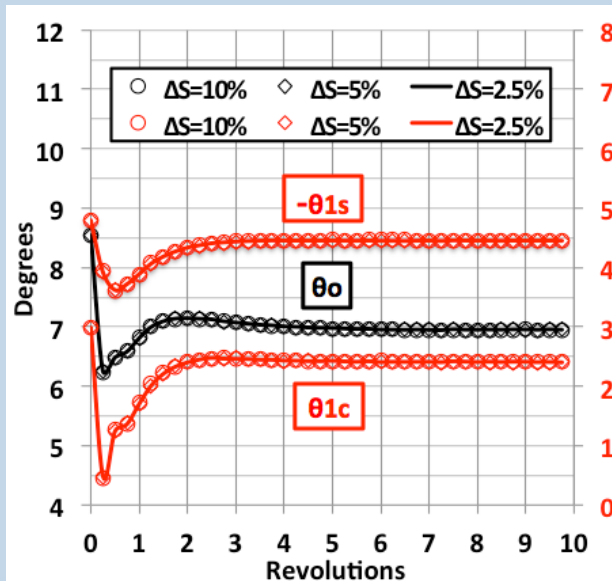
Loose Coupling Convergence History

BVI Flight Counter C8513

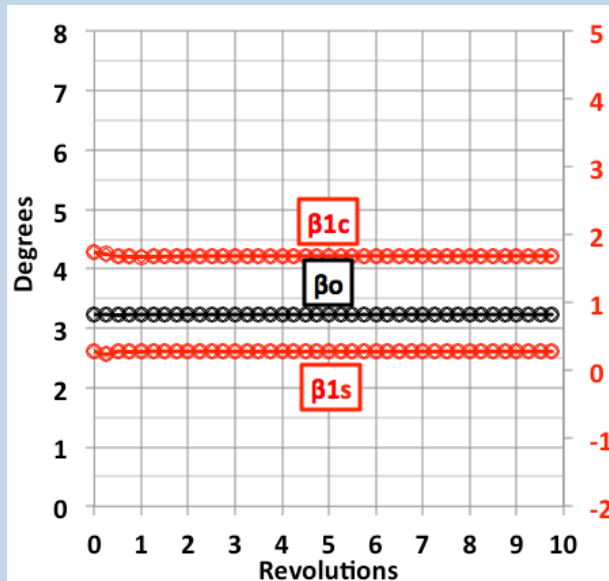
Blade Root Control Angles

$$\begin{pmatrix} \text{Pitch} \\ \text{Flap} \\ \text{Lag} \end{pmatrix} = \begin{pmatrix} \theta \\ \beta \\ \zeta \end{pmatrix} = \begin{pmatrix} \theta_o + \theta_{1c} \cos \psi + \theta_{1s} \sin \psi \\ \beta_o + \beta_{1c} \cos \psi + \beta_{1s} \sin \psi \\ \zeta_o + \zeta_{1c} \cos \psi + \zeta_{1s} \sin \psi \end{pmatrix}$$

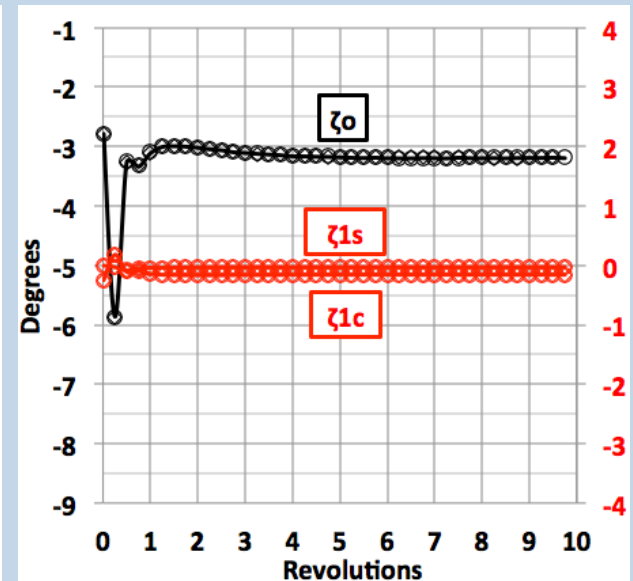
Pitch Angle



Flap Angle



Lag Angle

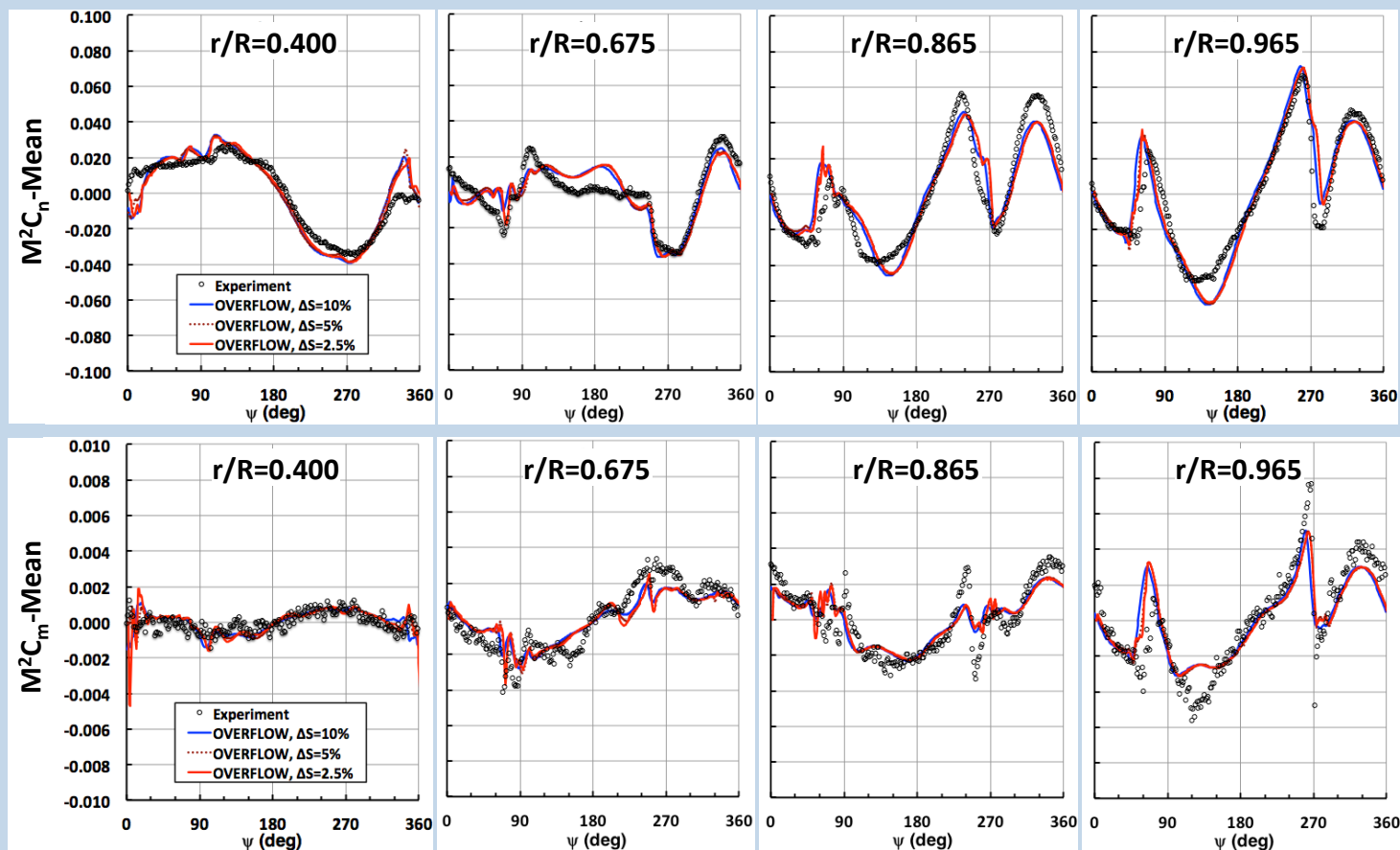




Effect of Wake-Grid Resolution on Airloads

BVI Flight Counter C8513

- Good overall agreement with flight-test data
- OB resolution has very little effect on airloads!





Outline

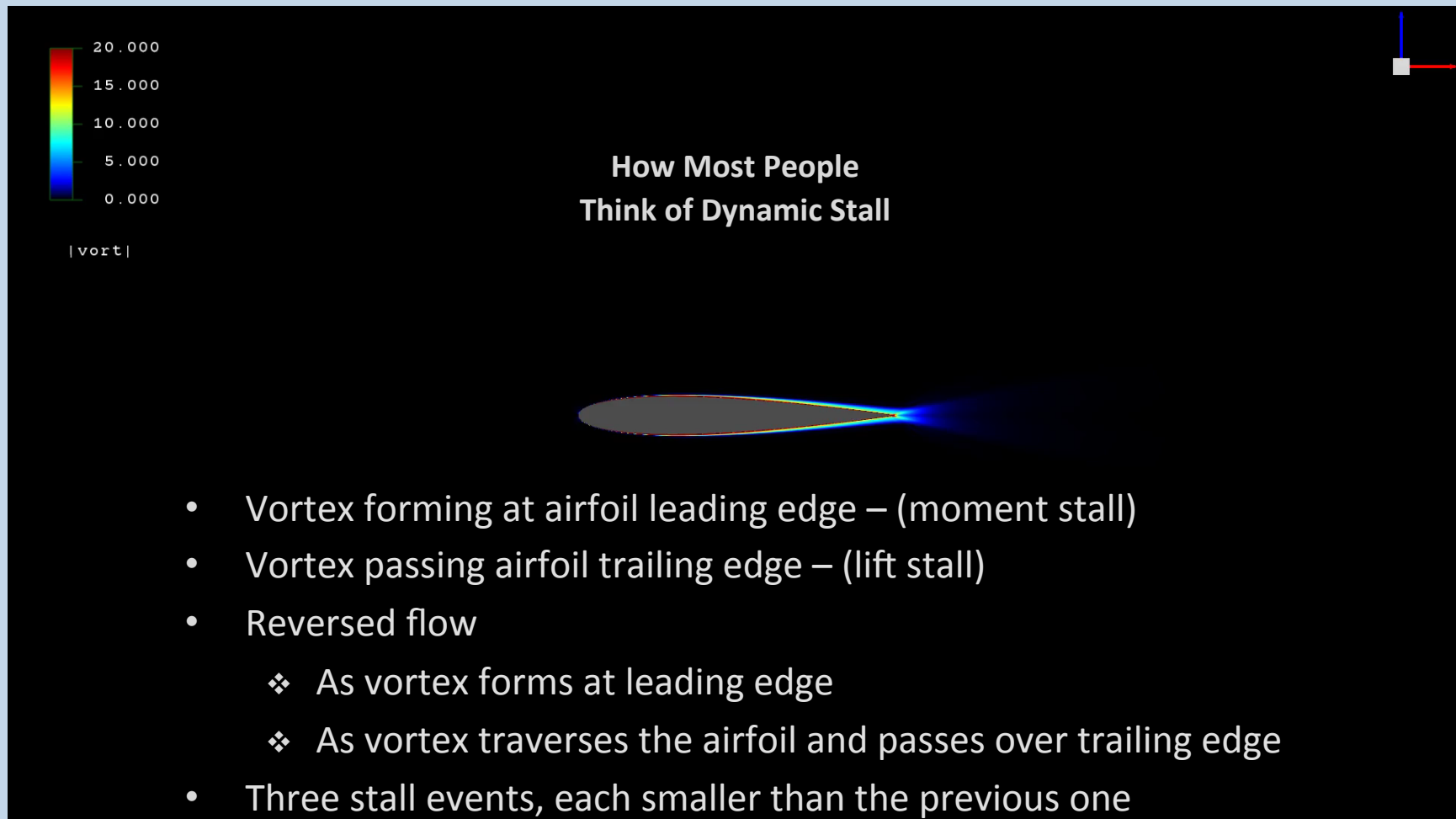
- Flight-Test Data
- Numerical Approach
- Numerical Results
 - ❖ BVI – UH-60A (C8513)
 - ❖ **Dynamic stall**
 - **2D example**
 - 3D UH-60A (C9017)
- Concluding Remarks



CFD Animation of Two-Dimensional Dynamic Stall



$$\alpha = 10^\circ + 10^\circ \sin(2kt - \frac{\pi}{2}), k = \frac{\omega c}{2V_\infty} = 0.1$$

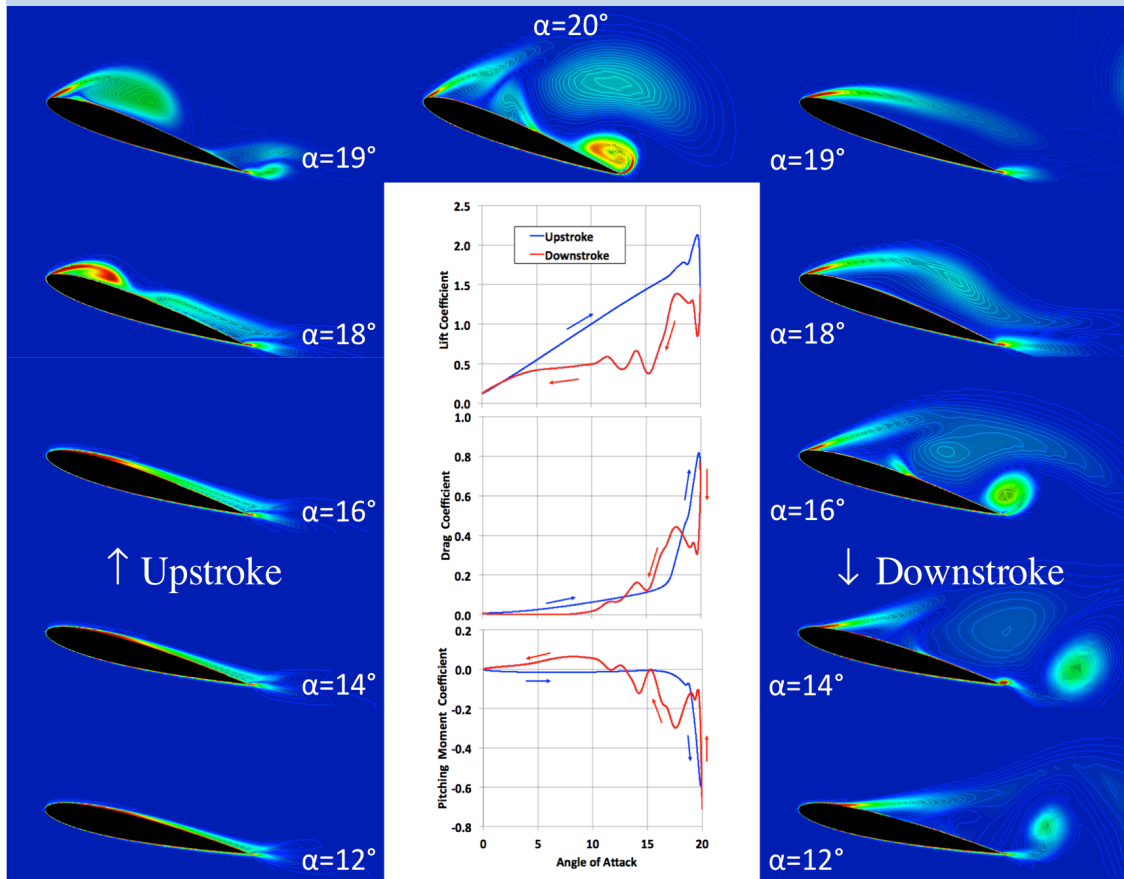




Two-Dimensional Dynamic Stall



$$\alpha = 10^\circ + 10^\circ \sin(2kt - \frac{\pi}{2}), k = \frac{\omega c}{2V_\infty} = 0.1$$



- Force/moment time-history indicates 3 stall events
 - ❖ 2-3 typical
 - ❖ 2D characteristics identified experimentally (McCroskey et al., 1976)
 - ❖ Many feel 2D captures the essential elements (Tan & Carr, 1996)
 - ❖ It will be shown that 2D does miss some important 3D dynamic stall characteristics



Outline

- Flight-Test Data
- Numerical Approach
- Numerical Results
 - ❖ BVI – UH-60A (C8513)
 - ❖ **Dynamic stall**
 - 2D example
 - **3D UH-60A (C9017)**
- Concluding Remarks



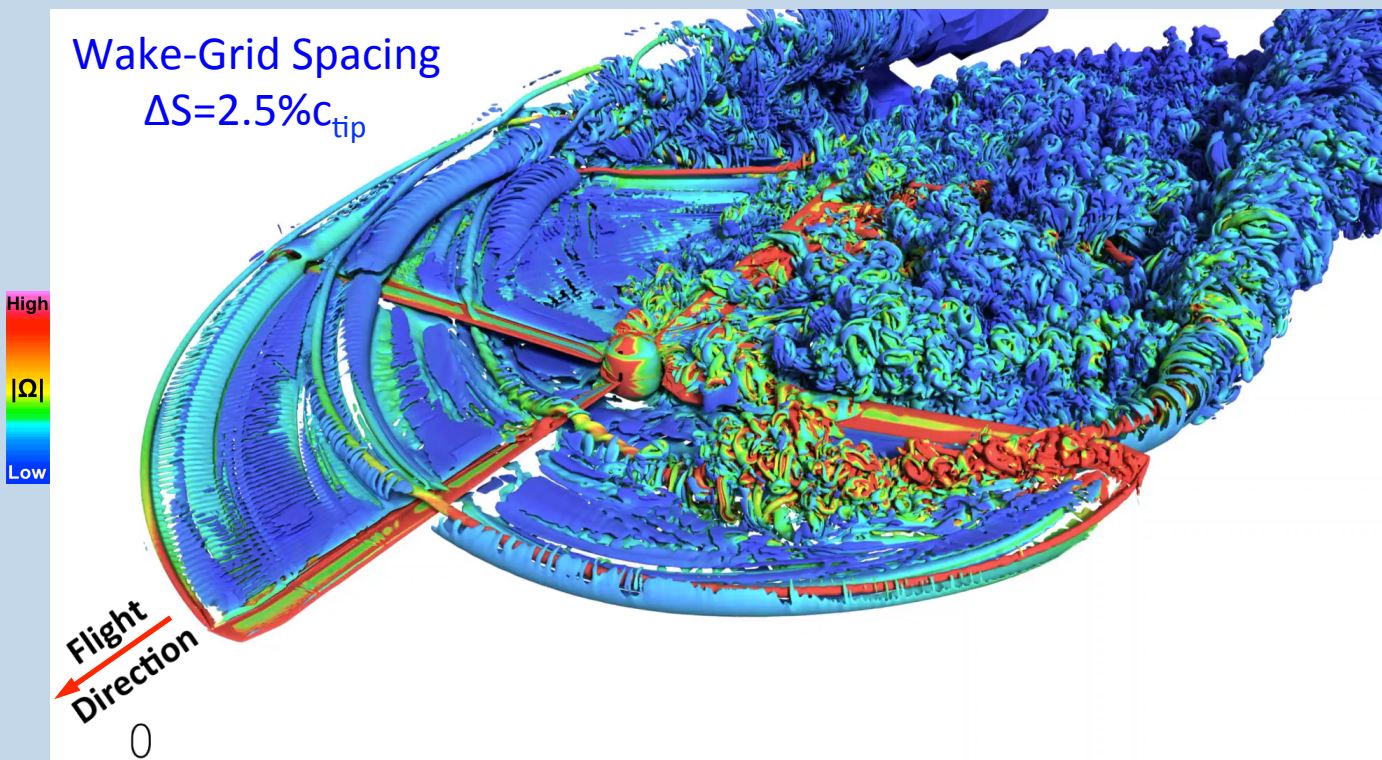
High-Resolution Dynamic Stall (C9017) NASA'S OVERFLOW Navier-Stokes CFD Code



M_∞	M_{tip}	μ	Re_{tip}	a_{shaft}, deg	b, deg	C_T
0.158	0.666	0.237	4.62×10^6	-0.15	-1.58	0.0110

There is BVI

It is affecting the dynamic stall process

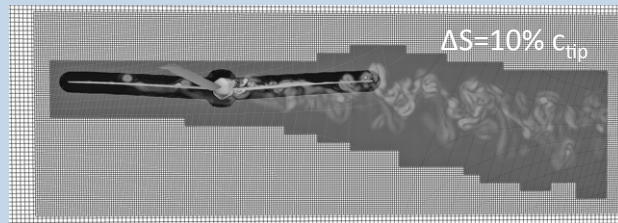




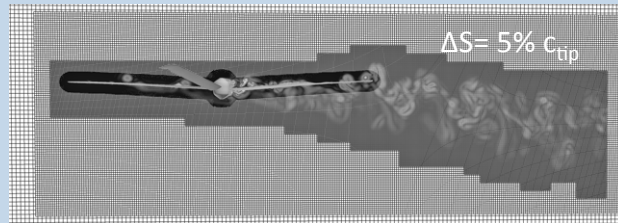
Three AMR Wake-Grid Resolutions

BVI Flight Counter C9017

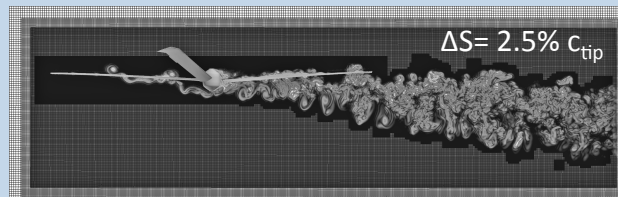
NASA's Pleiades Supercomputer
5,628 Broadwell CPU Cores



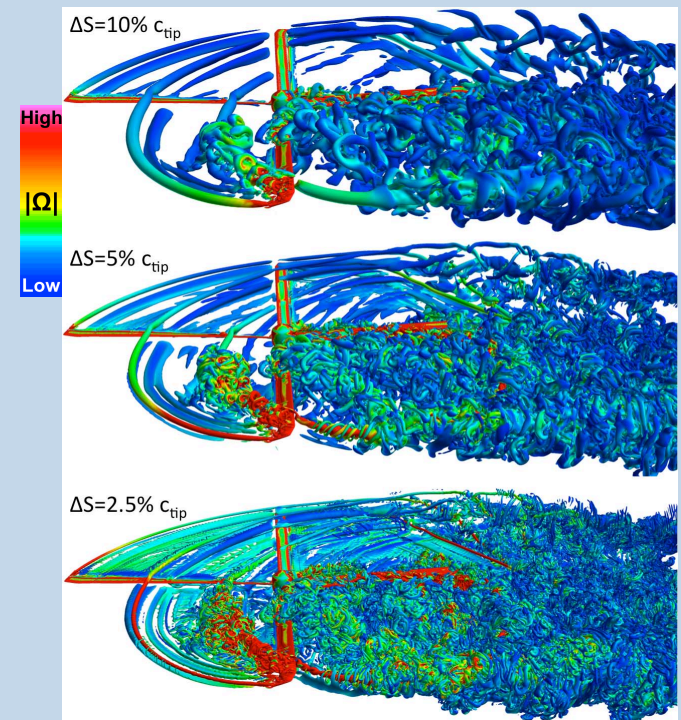
760 Grids
83 Million Grid Points
4.5 Hr/Rev



3,200 Grids
241 Million Grid Points
6.2 Hr/Rev



14,700 Grids
1.3 Billion Grid Points
28.5 Hr/Rev





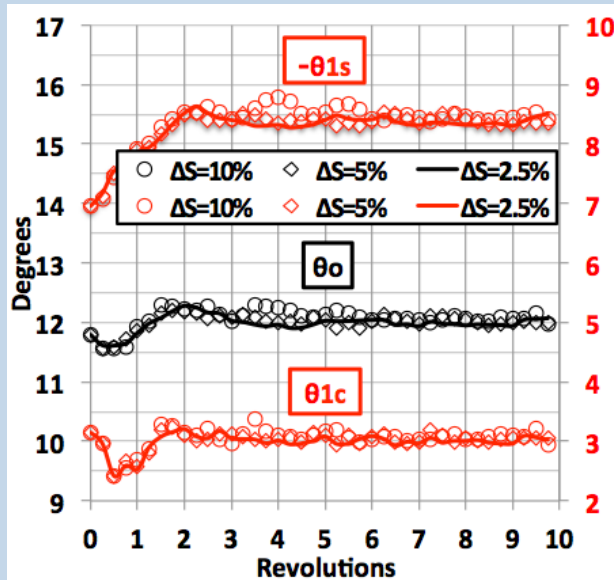
Loose Coupling Convergence History

BVI Flight Counter C9017

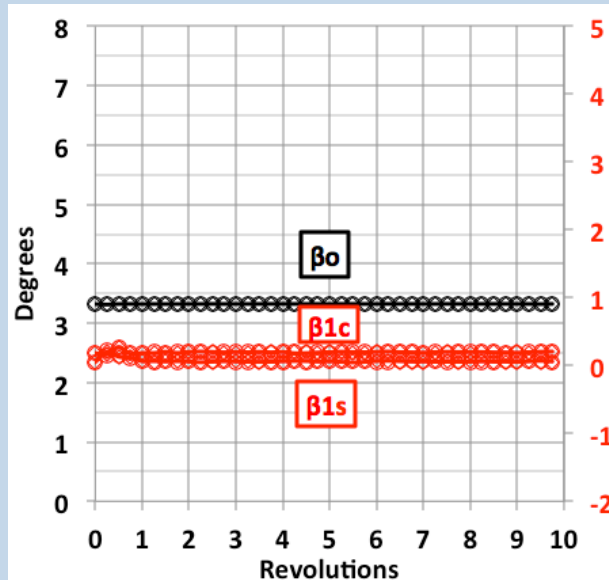
Blade Root Control Angles

$$\begin{pmatrix} \text{Pitch} \\ \text{Flap} \\ \text{Lag} \end{pmatrix} = \begin{pmatrix} \theta \\ \beta \\ \zeta \end{pmatrix} = \begin{pmatrix} \theta_o + \theta_{1c} \cos \psi + \theta_{1s} \sin \psi \\ \beta_o + \beta_{1c} \cos \psi + \beta_{1s} \sin \psi \\ \zeta_o + \zeta_{1c} \cos \psi + \zeta_{1s} \sin \psi \end{pmatrix}$$

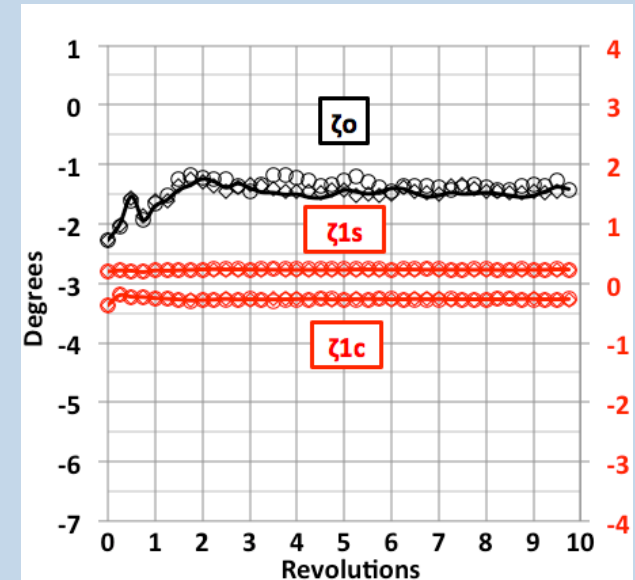
Pitch Angle



Flap Angle



Lag Angle



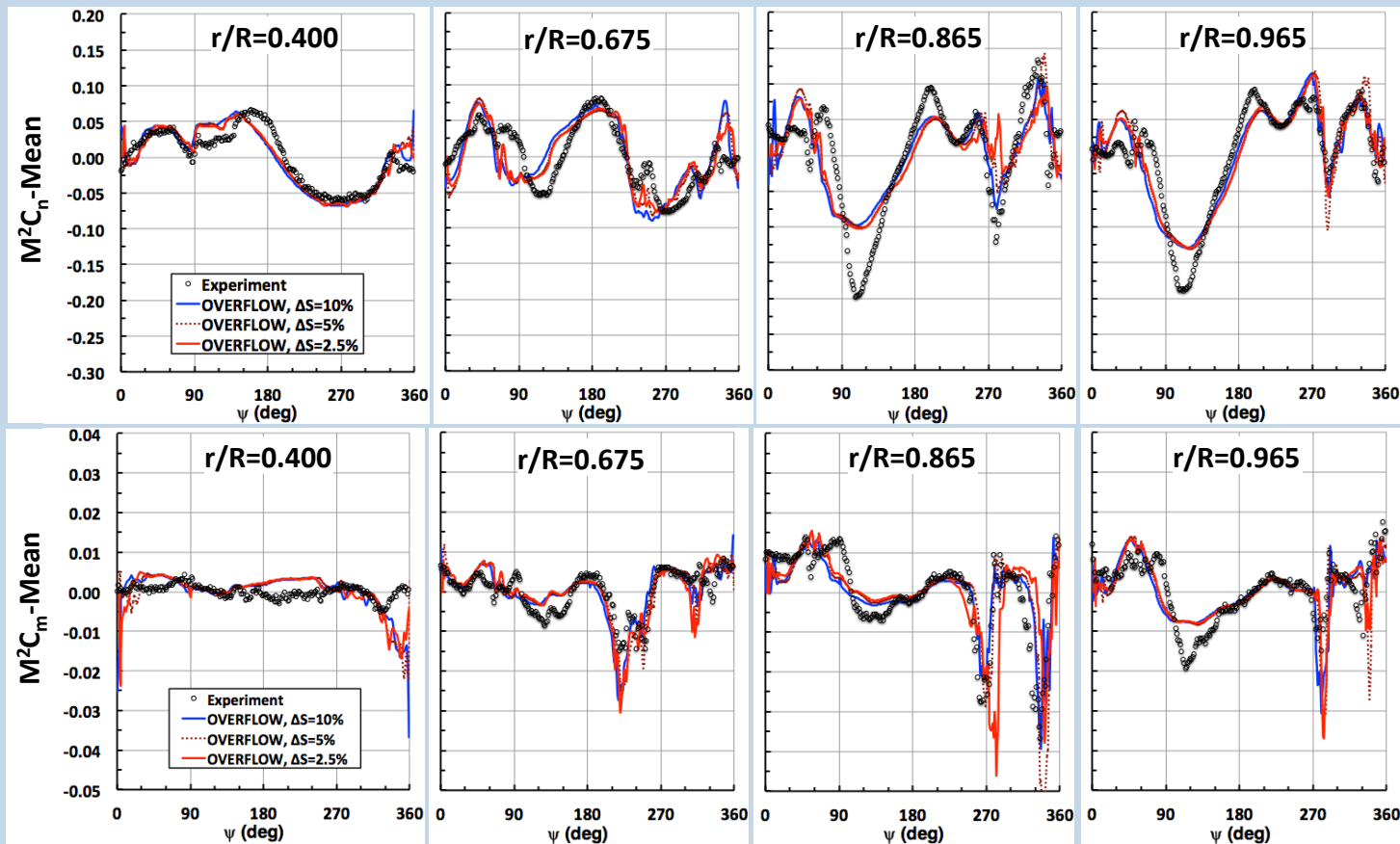


Effect of Wake-Grid Resolution on Airloads

Dynamic Stall Flight Counter C9017



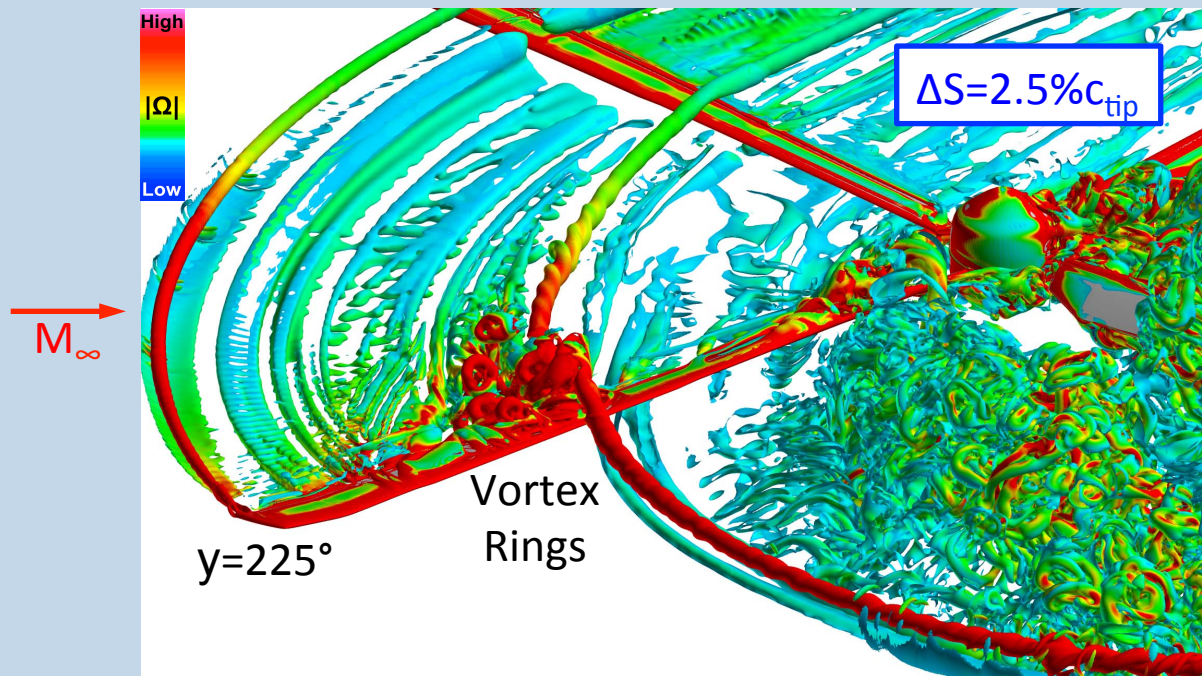
- Good overall agreement with flight-test data
- More high-frequency content, but little effect on airloads!
- This suggests $\Delta S=10\%c_{tip}$ adequate for engineering design airloads





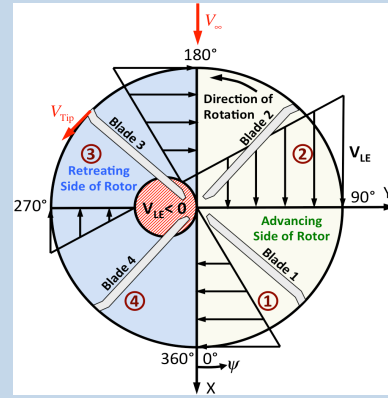
Closeup View of 3D Dynamic Stall With BVI

- Inboard and outboard separation, with attached flow in between
- 3D Vortex rings emitted due to Helmholtz vortex theorem
 - ❖ Different from 2D Vortex lift-off
- Vortex path altered due to separation
 - ❖ Can effect aeromechanics of following rotor blades





Closeup View of Dynamic Stall

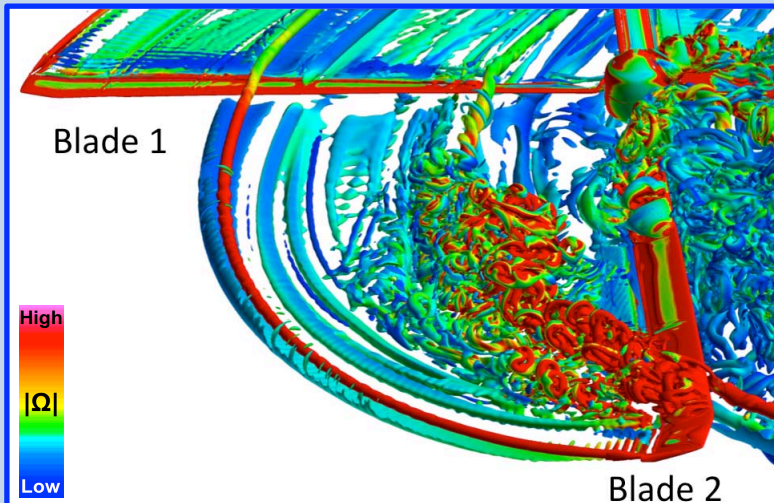


Nomenclature

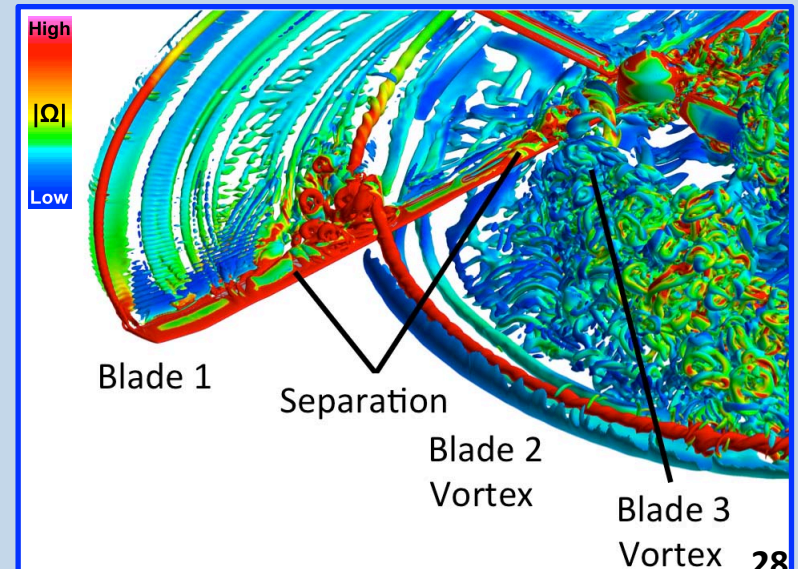
- Tip vortices from Blades 2 and 3 do not disrupt the flow on Blade 1

- Flow separates outboard of vortex, remains attached inboard of vortex
- Separation moves with the vortices
- Tip vortices from Blades 2 and 3 appear to trigger dynamic stall

Blade 1 at $y=180^\circ$



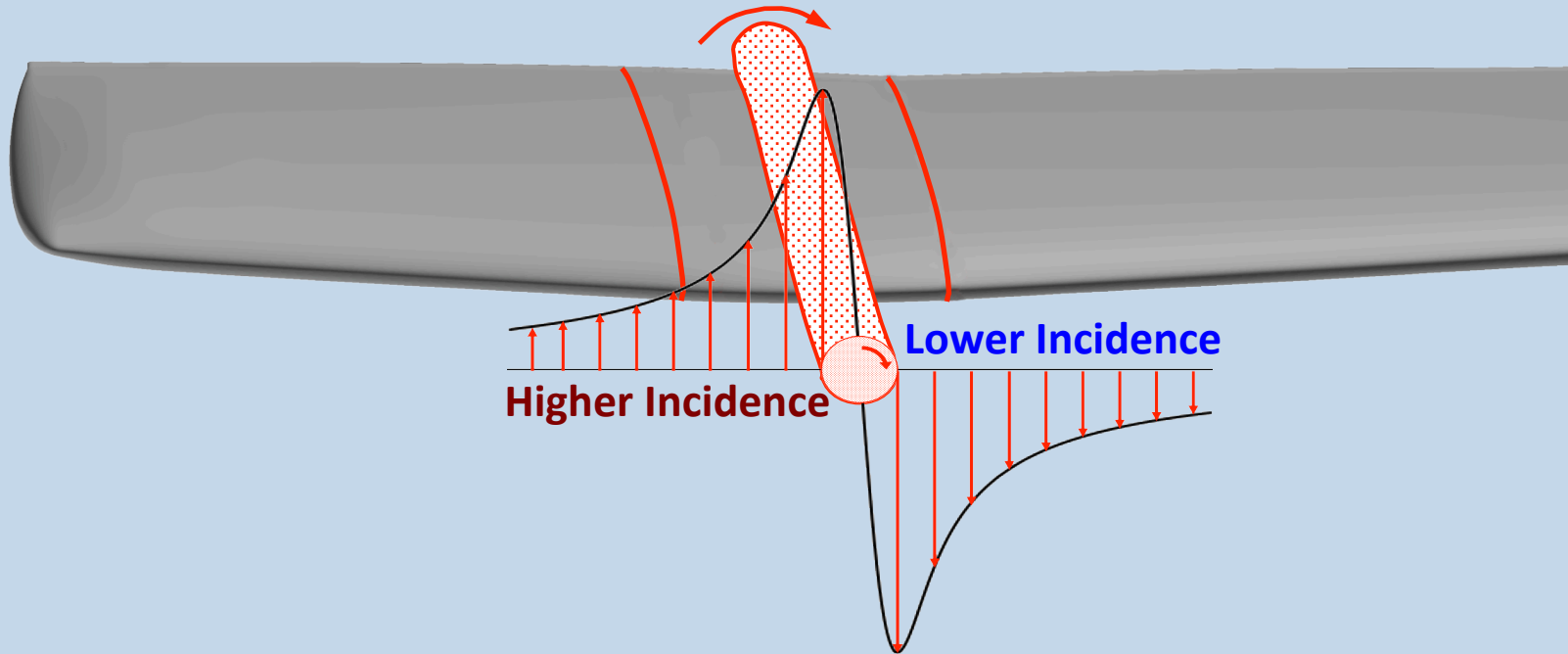
Blade 1 at $y=225^\circ$





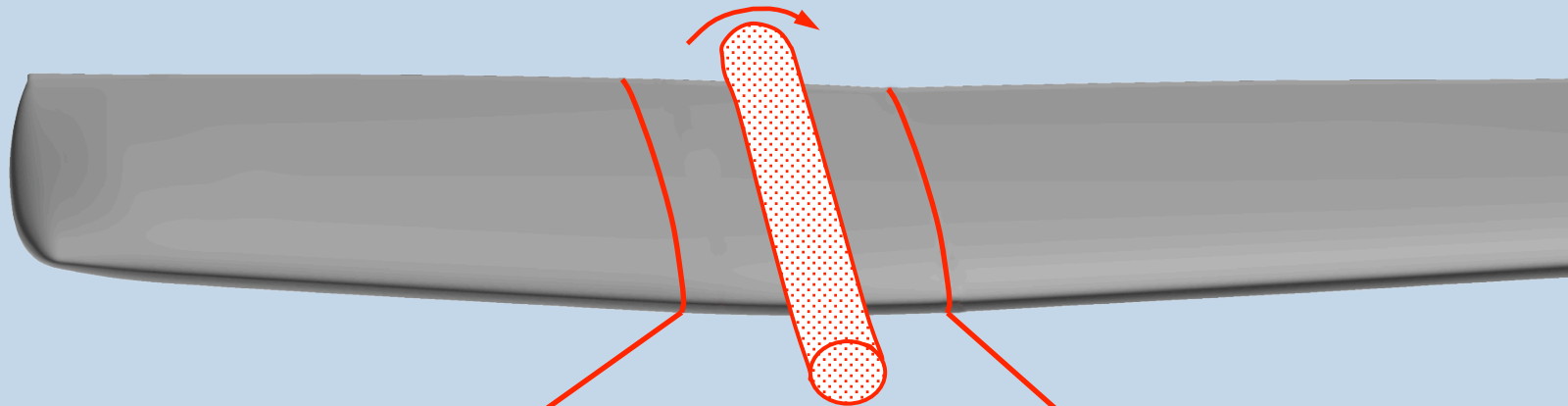
Rotating Blackhawk Rotor Blade

But What Happens When a Vortex Passes Over the Blade?

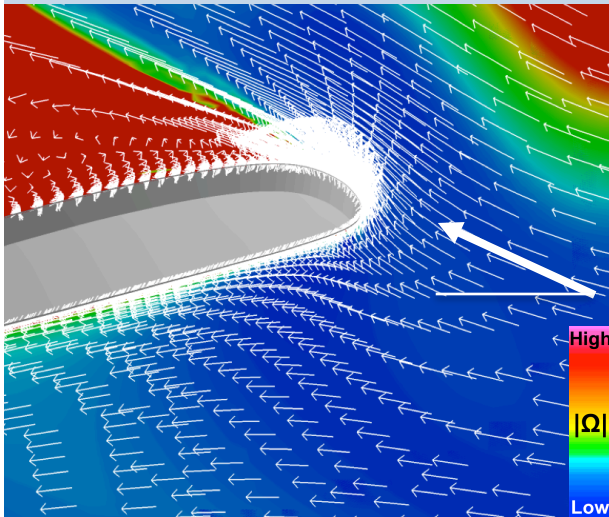




Velocity Vectors Relative to Rotor Blade

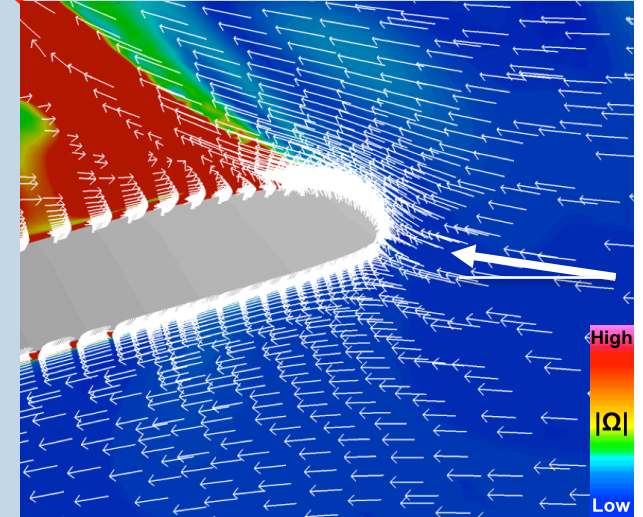


Outboard of Vortex



- Outboard incidence is greater than inboard incidence by at least 10 deg
- This explains why stall occurs outboard of the vortex and reattaches inboard of the vortex

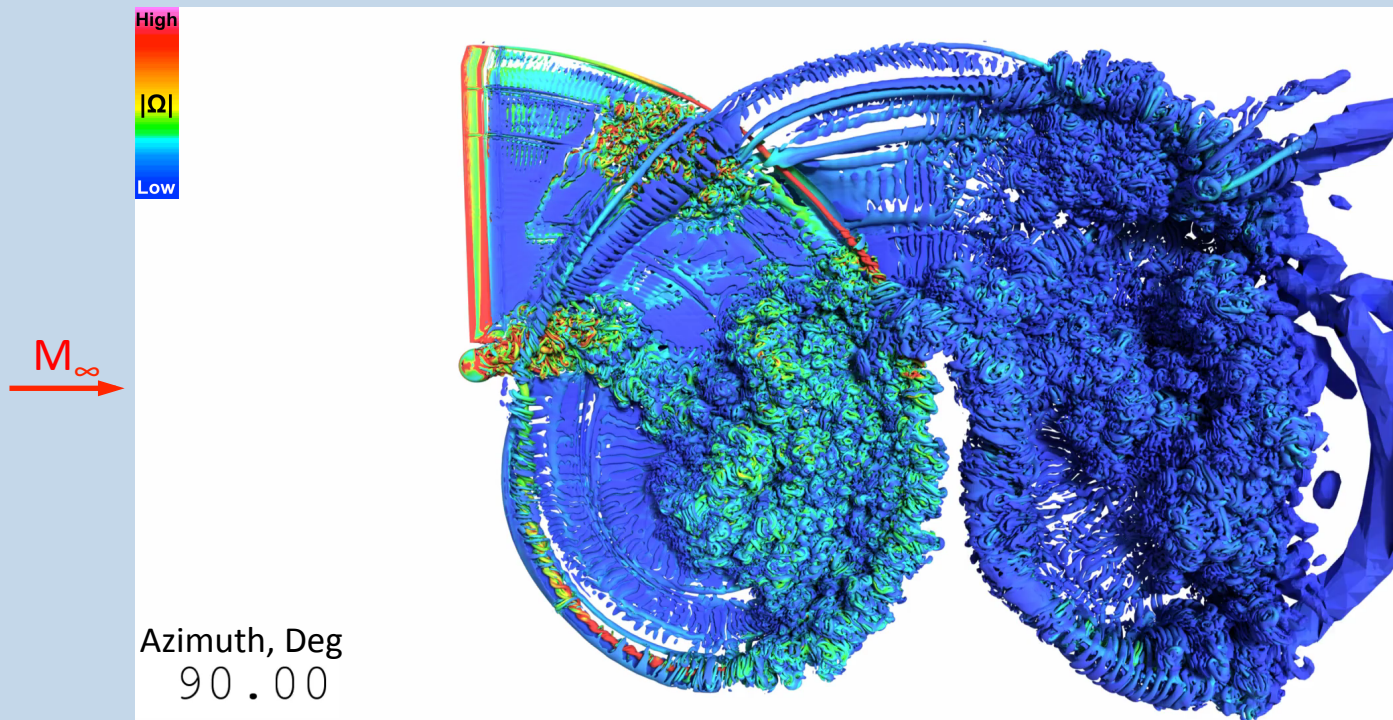
Inboard of Vortex





Closeup View of a Single Blade (Same Blade Motion and Aeroelastic Deflections)

- No outboard separation in the 3rd quadrant!
 - ❖ **This confirms vortex-induced dynamic stall**
- Inboard separation due to freestream reversed flow
- Separation along entire blade in 4th quadrant, due to blade incidence

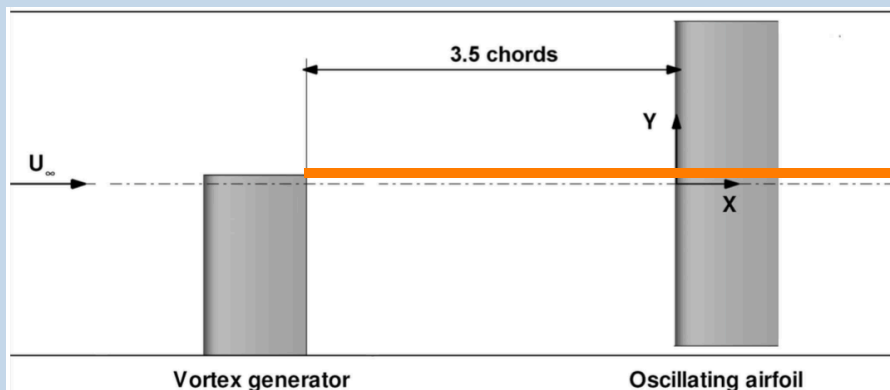




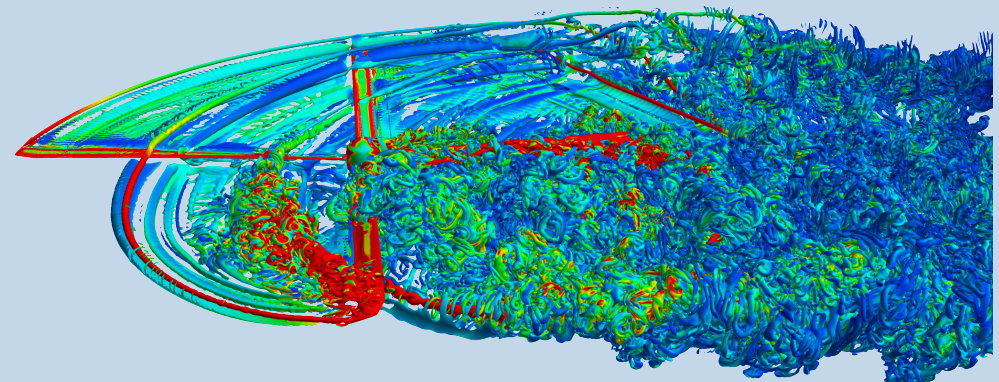
BVI-Induced Dynamic Stall (C9017)

- This phenomenon is virtually unknown throughout the rotorcraft community
- First observed in a 2D airfoil experiment
 - ❖ 38th European Rotorcraft Forum: Zanotti, Gilbertini and Mencarelli
 - ❖ Similar explanation of how a vortex triggers dynamic stall
- Also presented at the 73rd AHS Forum (May 2017)
 - ❖ Francois Richez: Computational analysis for a rotor wind tunnel experiment
 - ❖ Neal Chaderjian: First time observed for an actual helicopter rotor in flight
- CFD is used to provide greater detail and insight than available in the experiment

2D Wind-Tunnel Experiment



3D UH-60A Rotor

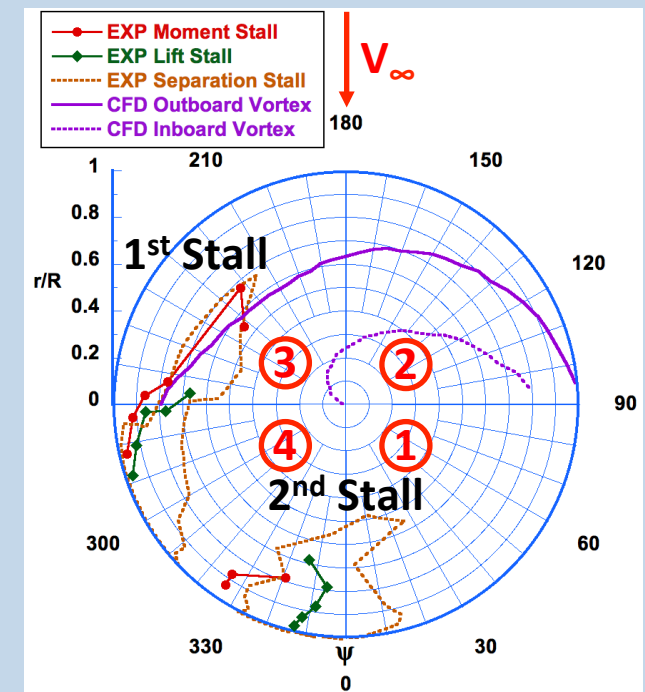




Comparison of CFD With Qualitative Flight-Test Analysis (Dynamic Stall, C9017)



- Polar plot
 - ❖ Bousman's **moment stall**, **lift stall**, and **trailing-edge separation**
 - ❖ There are two stall events
 - ❖ CFD Outboard and inboard vortices
 - Outboard vortex initially moves inboard then outboard
 - ❖ Tracks stall closely up to 270°, where it drops below the blade and has little influence
 - ❖ Inboard vortex only moves inboard
- Flight test does not indicate inboard reversed flow
 - ❖ It must be there, but loads are light and pressure data sparse (Bousman)





Time-Dependent Flow Visualization of Dynamic Stall Blackhawk Helicopter Rotor in Forward Flight

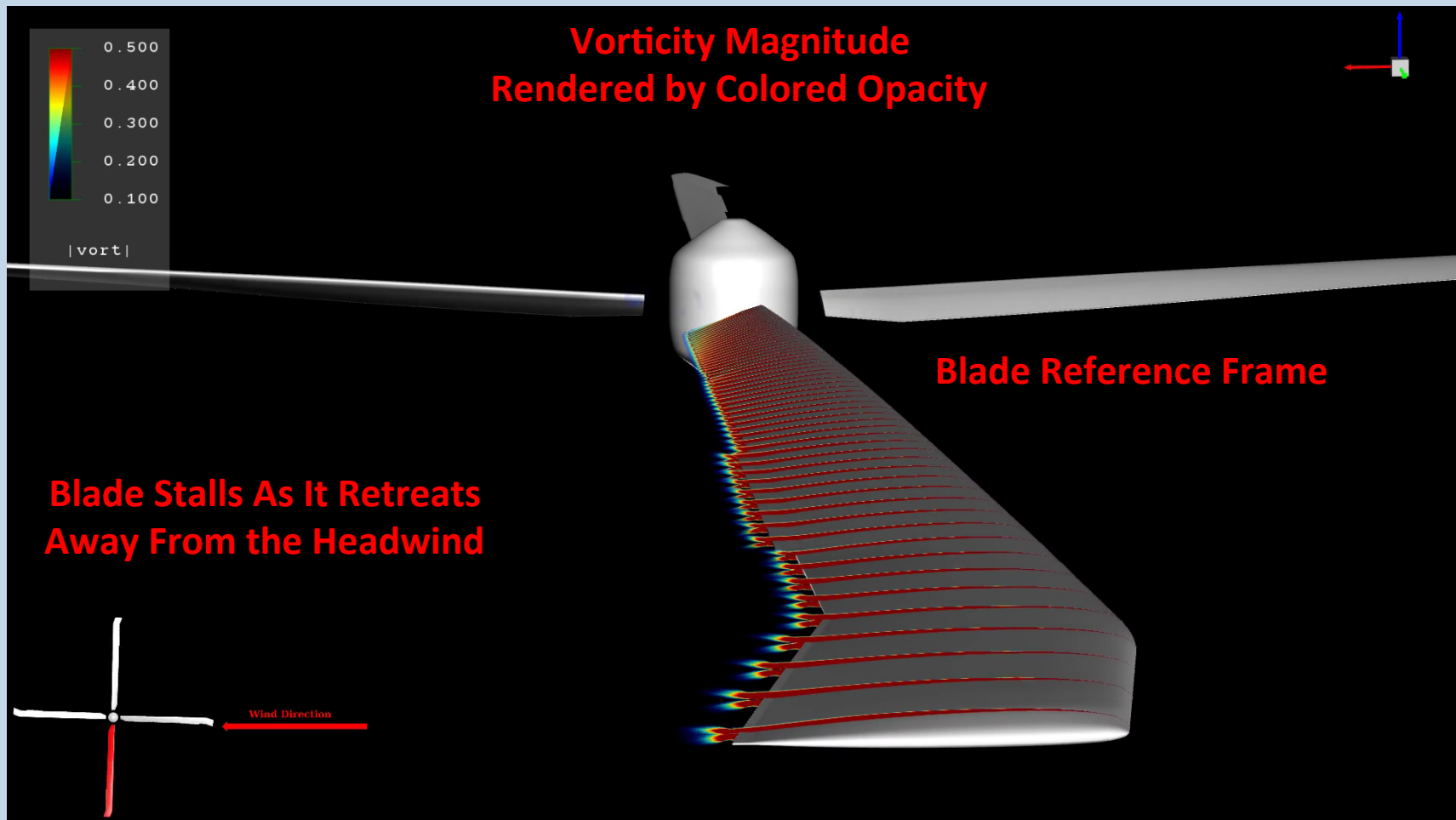
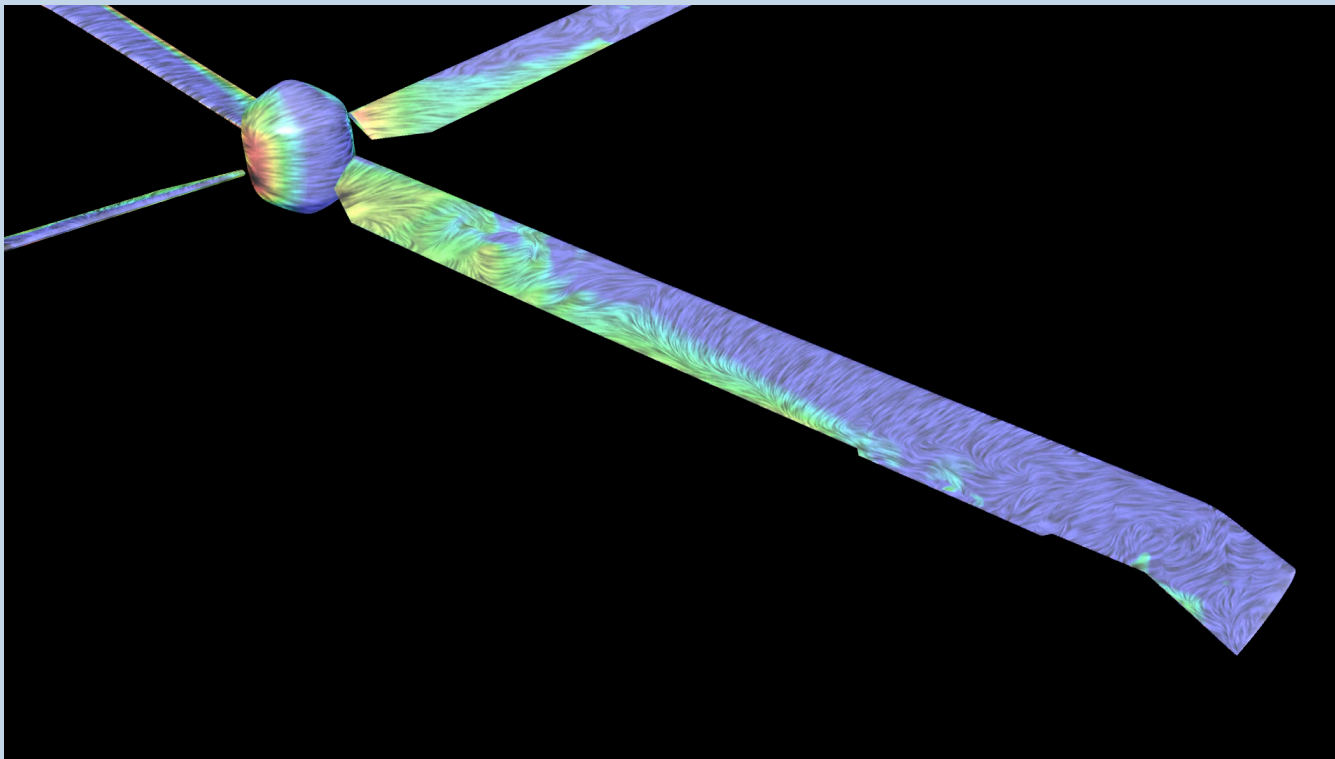




Image Based Flow Visualization (IBFV)

- Time depended surface flow using a IBFV technique
- Colored by pressure (Red->High; Blue->Low)
- Dark lines show flow separation and reattachment





Conclusions

- Good overall comparison between CFD airloads and flight-test measurements for BVI and dynamic stall cases
 - wake grid resolutions were $\Delta S=10\%$, 5% , and $2.5\% C_{tip}$
- Refining rotor wakes beyond engineering resolution ($\Delta S=10\% C_{tip}$) did not significantly affect the predicted airloads, even with blade/wake interaction
 - ❖ This suggests that airloads engineers may use the coarser wake-grid resolution ($\Delta S=10\%c_{tip}$) for hover and forward flight simulations provided
 - The CFD tip-vortex is accurately formed using a combination of fine surface mesh at the blade tip and high-order spatial accuracy
 - Use of a hybrid RANS/DDES turbulence model
 - ❖ No statement is inferred for acoustics
 - High frequency content was observed on the higher-resolution rotor wakes



Conclusions (Continued)

- ❖ Differences between 2D and 3D dynamic stall
 - 3D vortex rings are emitted rather than a simple 2D leading-edge vortex
 - Dynamic stall flow separation can alter the path of a BVI vortex
 - Vortices passing over the rotor blade caused BVI which triggered dynamic stall
 - ❖ This phenomenon has been observed in a 2D wind-tunnel experiment and also 3D rotor simulations (73rd AHS Forum)
 - Mechanism for BVI-triggered dynamic stall
 - ❖ Induced velocity field by other blade-tip vortices changed the relative angle of attack of the stalling rotor blade
 - The blade AOA increased outboard of the BVI vortex, causing flow separation
 - The blade AOA decreased inboard of the BVI vortex, resulting in attached flow
- ❖ The successful modeling of 3D dynamic stall with BVI should include an accurate prediction of blade-tip vortex trajectories



Acknowledgements

- Mr. Tim Sandstrom for truly state-of-the-art time-dependent flow visualization
- Mr. Bill Bousman for his helpful discussions of the UH-60A flight test
- NASA's RVLT Program for supporting this work
- NASA's Advanced Supercomputing (NAS) Division (Pleiades Supercomputer)

